Article:
Zeng, Y, Liang, G, Qiang, B et al. (10 more authors) (2018) Two-Dimensional Multimode Terahertz Random Lasing with Metal Pillars. ACS Photonics, 5 (7). pp. 2928-2935.

https://doi.org/10.1021/acsphotonics.8b00260

Two-Dimensional Multimode Terahertz Random Lasing with Metal Pillars

Yongquan Zeng[1], Guozhen Liang[1], Bo Qiang[1], Kedi Wu[1], Jing Tao[1], Xiaonan Hu[1], Lianhe Li[2], Alexander Giles Davies[2], Edmund Harold Linfield[2], Hou Kun Liang[3], Ying Zhang[3], Yidong Chong[4], and Qi Jie Wang[1,4,*]

[1] Centre for OptoElectronics and Biophotonics, School of Electrical and Electronic Engineering, Nanyang Technological University, 50 Nanyang Avenue, Singapore 639798, Singapore

[2] School of Electronic and Electrical Engineering, University of Leeds, Leeds LS2 9JT, UK

[3] Singapore Institute of Manufacturing Technology, 2 Fusionopolis Way, Singapore 138634, Singapore

[4] School of Physical and Mathematical Sciences, Nanyang Technological University, 21 Nanyang Link, Singapore 637371, Singapore

*Email: qjwang@ntu.edu.sg

Abstract

Random lasers employing multiple scattering and interference processes in highly disordered media have been studied for several decades. However, it remains a challenge to achieve broadband multimode random laser with high scattering efficiency, particularly at long wavelengths. Here, we develop a new class of strongly multimode random lasers in the terahertz (THz) frequency range in which optical feedback is provided by multiple scattering from metal pillars embedded in a quantum cascade (QC) gain medium. Compared with the dielectric pillars or air hole approaches used in previous random lasers, metal pillars provide high scattering efficiency over a broader range of frequencies and with low ohmic losses. Complex emission spectra are observed with over 25 emission peaks across a 0.4 THz frequency range, limited primarily by the gain bandwidth of the QC wafer employed. The experimental results are corroborated by numerical simulations which show the lasing modes are strongly localized.

TOC Graphic:

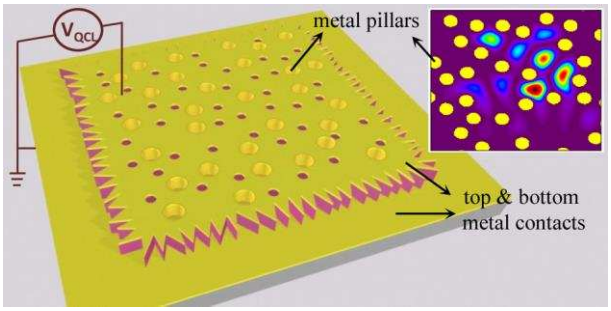

Keywords: random laser, terahertz frequency, quantum cascade laser, multimode lasing, localization

Random lasers[1,2] are a special class of laser in which the lasing modes are confined by the multiple scattering of light from randomly-placed scatterers, rather than by a well-defined optical cavity. Such lasers are host to a number of complex and intriguing physical phenomena such as mode localization and de-localization[3,4], complex gain competition and mode coupling[5,6], and strong light-matter interactions[7,8]. To date, researchers have achieved random lasing in a wide range of random media including nanocrystalline ZnO powders[9,10], ceramics[11], organic composites[12], air holes drilled into semiconductor membranes[13], fibre cores[14], and nanoparticles (e.g., TiO_2, ZnO, GaN, gold/silver nanoscatterers, and even graphene nanoflakes) dispersed in fluorescent dyes[1,15–18]. In addition to the fundamental scientific interest, random lasers are highly promising sources of broadband, low spatial coherence yet high intensity illumination, with promising applications in display lighting, biological probes[19], and optical imaging[20].

Electrically-pumped random lasers based on quantum cascade (QC) heterostructures have recently been developed[21–24]. Operating at mid-infrared or terahertz (THz) frequencies, these devices consist of randomly-distributed air holes[21,22] or dielectric pillars[23,24] fabricated from QC wafers. In particular, THz quantum cascade lasers (QCLs) consisting of QC pillars embedded in a low-index polymer have

been shown to exhibit multi-mode emission and strong mode localization[24]– key features required for a low spatial coherence light source. A typical device based on this design exhibited thirteen random lasing peaks, emitted from a 1000 μm × 1000 μm area in the frequency range of 3.1 – 3.4 THz. The operating frequency range coincided with a "lower band edge" adjacent to a spectral pseudo-gap, where modal quality (Q) factors were strongly enhanced. This aspect of the design imposed a fundamental limit on the frequency bandwidth of the multi-mode random laser.

In this paper, we report on the design and implementation of a new type of electrically-pumped THz random QCL, in which the structures comprise metal (Au) pillars embedded at random positions in the QC wafer. Unlike the previous design that used dielectric pillars, metal pillars are able to sustain high Q factors over a much broader frequency range, extending over several THz above the cutoff frequency[25]. At these frequencies, the metal pillars have extremely high scattering efficiencies (comparable to, or exceeding, those of dielectric pillars with three times the radius; see **Figure 1b**), allowing for the strong confinement of the random laser modes, whereas the ohmic losses are essentially negligible. We are thus able to demonstrate ≥ 25 lasing peaks from a ~ 500 μm × 500 μm sample: i.e., twice the number of peaks from a quarter of the area compared to our previously-reported THz random QCL[24]. These lasing peaks are presently limited to a range of approximately 0.4 THz, determined by the gain bandwidth of the QC wafer. By using QC wafers with larger gain bandwidths[26], it will be possible to achieve ultra- broadband random lasing (~ 1 THz).

There have been a number of studies of metallic photonic crystals comprising metal pillars arranged in an ordered two-dimensional (2D) lattice. Such structures can produce an exceptionally broad photonic band gap ranging from zero frequency to a cutoff frequency, usually at GHz to THz scales, with interesting applications for RF-scale waveguides, filters, polarizers, and other devices[25,27]. Bayindur et al.[28] have shown that in disordered lattices of metal pillars, the low-frequency band gap is

extremely robust against disorder, and the power spectrum is elevated in a broad frequency range above the gap. However, systematic research on the scattering property of individual metal pillar, optical cavities and experimental demonstration of photonic active devices with disordered metal pillar lattices have not been reported yet to the best of our knowledge.

Here, it is found that disordered lattices of metal pillars have excellent optical properties and are superior to the widely used random structures, e.g. random dielectric pillar structure and random air hole structure, for the application of THz random lasers. **Figure 1a** shows the simulated 2D transverse-magnetic (TM) optical power spectrum of a disordered lattice of circular Au pillars embedded in GaAs (representing the QC wafer medium). For comparison, we also show simulated results for two other random structures corresponding to previously reported random QCLs: dielectric pillars (GaAs) in a benzocyclobutene (BCB) polymer background[24], and air holes in a GaAs background[22]. The structures each comprise 680 scatterers (Au pillar, dielectric pillar, or air holes), randomly distributed in a region of 500 μm × 500 μm. An identical random placement is used for each structure. The circular scatterers have different radii R, with R = 4 μm for the Au pillars, and R = 6.4 μm for the dielectric pillar and the air holes. The positions of the scatterers are determined by a random placement algorithm with the same placement constraint used in Ref. 24 to generate short-range order. It is worth to mention that the scatterer position generation method and the scatterer size are optimized for dielectric pillar structure in the application of multimode localized random lasing around 3 THz range (see Ref. 24 and SI Text, Figure S1 and Figure S3). The refractive index of GaAs is taken to be 3.60, the refractive index for BCB is 1.58, and the complex dielectric function of Au is

$$\varepsilon_{\mathrm{c}} = \varepsilon_{\infty} - \frac{\omega_{\mathrm{p}}^2}{\omega^2 + \mathrm{i}\omega\omega_{\tau}} \tag{1}$$

where ω_p = 1.37× 10^{16} rad/s is the plasma frequency, τ = 0.15 ps is the Drude scattering time, and ε_∞ = 1 is the high-frequency limit of the dielectric constant; these are standard values based on a parameter fit in the far-infrared frequency range[29]. To calculate the power spectrum, 2D finite-difference time-domain (FDTD) simulations were used. In the simulations, randomly distributed multiple dipoles were used to inject Gaussian pulses into the structure. Time evolutions of the electric field at different positions were recorded and summed before being Fourier transformed[30]. It was focused on TM polarization because QCLs (unlike traditional semiconductor diode lasers) emit with this polarization[31].

The results in **Figure 1a** show that the disordered lattice of Au pillars has a spectral gap at low frequencies. Over a broad range (≥ 3 THz) above the gap, the spectrum is dominated by numerous high-Q resonance peaks. It will be shown in **Figure 2** that the corresponding resonant modes are strongly localized. Owning to the interplay between Mie resonances and short-range order, the dielectric pillar structure supports pseudo-gaps at ~ 3.5 THz and ~ 6 THz (not so obvious due to the weak short-range order)[24]. High-Q "bandedge" resonance peaks with localized modal profiles can only be found in its spectrum (vertically shifted down by 10^3 a.u. for clarity) over a significantly narrower frequency range lying below the pseudo-gaps. As for the air hole structure, its spectrum (vertically shifted down by 10^6 a.u. for clarity) is relatively featureless and the typical resonant modes are extended, which can be attributed to the poor scattering efficiency of air holes for TM polarization[24]. For further discussions of the optical property of the metal pillar and dielectric pillar structures, see SI Text, Figure S1-S3.

To unveil the theoretical basis and further outline the advantages of the disordered metal pillar lattice, **Figure 1b** compares the scattering efficiency of individual scatterer in each of the three cases: an Au pillar in GaAs, a GaAs pillar in BCB, and an air hole in a GaAs background. Here, the scattering efficiency (Q_{sca}) is defined as the dimensionless ratio of the total scattering cross section (which, in 2D,

has units of length) to the pillar diameter. These numerical results were obtained by partial-wave analysis (see **Methods**). It can be observed that the scattering efficiencies of the dielectric pillars vanish at low frequencies; at higher frequencies, they exhibit a series of broad peaks (the Mie resonances), the lowest occurring at around 3 THz. By contrast, the scattering efficiencies of the Au pillars diverge at low frequencies, and decrease with increasing frequency within the plotted range, with pillars of smaller radius having a higher scattering efficiency. Below around 3 THz, their scattering efficiencies exceed those of the dielectric pillars. The scattering efficiencies of the air holes are substantially lower than the other two types of scatterer.

The divergence of the scattering efficiency of metal pillars at low frequencies is consistent with Mie theory, which states that the scattered far-field profile for a cylinder of a perfect electrical conductor is given, to the lowest order of the cylinder radius R, by[32]

$$E_z^s = E_0 \sqrt{\frac{\pi}{2kr}} \frac{1}{(\ln kR)^2} e^{ikr - i\pi/4} \tag{2}$$

where r is the distance from the center of the cylinder, E_0 is the amplitude of the incident wave, and k is the radiation wavenumber in the background medium. Thus, to the lowest order in R, the scattering efficiency is

$$Q_{sca} = \frac{\sigma_{sca}}{2R} = \frac{\pi^2}{2} \frac{1}{kR(\ln kR)^2} \tag{3}.$$

This diverges in the limit $kR \ll 1$, similar to the numerical results shown in **Figure 1b** (we emphasize, however, that the Au pillars are not assumed to be perfect conductors in **Figure 1b**).

The fact that Au pillars have high scattering efficiency at small radii is advantageous for random lasing. It allows a strongly-scattering random medium to be achieved with relatively low filling

fractions (FF) of Au pillars, so that the background QC gain medium occupies a larger relative area. The transport mean free path l_t can be estimated by[2]

$$l_t = \frac{1}{\rho\sigma_{sca}\left(1-\langle\cos\alpha\rangle\right)} = \frac{\pi R}{FF\times Q_{sca}\times\left(1-\langle\cos\alpha\rangle\right)} \quad (4)$$

where α is the scattering far-field angle for a single scatterer. For the Au pillar scatterer (R = 4 μm) at a frequency corresponding to free space wavelength of 100 μm, we estimated that $\langle\cos\alpha\rangle \approx 0.084$ by calculating the scattering far-field intensity distribution of a single Au pillar. This yields a transport mean free path of $l_t \approx 46$ μm for FF = 10%, much shorter than the system size (typical system size is ~ 500 μm in this work), indicating the strong localization property of the random structure.

The optical modes of 2D disordered Au pillar lattices have been studied via finite element method (FEM) simulations performed using the Comsol Multiphysics package. In these simulations, out-of-plane radiative losses were not accounted for, only the ohmic losses within the pillars and in-plane radiative losses from the sample edges. A perfectly matched layer was used to eliminate reflections from the simulation domain boundaries. The Au pillars have radius R = 4 μm, and are randomly distributed, without overlap, within a 500 μm × 500 μm region. We have studied several different FFs, ranging from 6% to 20%, solving for eigenmodes of the open system within the frequency range 2.95 THz – 3.45 THz (the gain width of the actual QCL wafer). To illustrate the intrinsic resonant property of the random structures, the optical gain was not considered in the calculations.

The results are shown in **Figure 2**. For low-FF structures (e.g. 6%), the typical optical mode extends over a broad area. With increasing FF, the modes become more confined; for 18% FF, each mode is strongly localized to within a few multiples of the mean inter-pillar separation, centered at a random part of the sample.

To quantify these observations, **Figure 2d** plots the mean Q factors, effective modal size L_{eff}, and ohmic loss rate as a function of pillar FF. The modal size is defined as[33]

$$L_{eff} \equiv \sqrt{\left[\int I(x,y)dxdy\right]^2 \Big/ \left[\int I(x,y)^2 dxdy\right]} \tag{5}$$

and serves as an estimate for the localization length scale. The Q factor of each optical mode is calculated by $Q = \omega_r / 2\omega_i$, where $\omega_r + i\omega_i$ is the complex eigenfrequency of the mode. The loss rate is defined as $2\omega_i / c$, where c is the velocity of light in the medium. All three quantities plotted in **Figure 2d** are obtained by averaging over the 150 highest-Q eigenmodes within the 2.95 THz – 3.45 THz frequency range, and for five independent sample configurations for each FF. From these results, it can be found that the Q factors increase with FF up to around 12% – 16%, before subsequently decreasing. This decrease can be attributed to increasing ohmic losses; to show this, the mean ohmic loss within the structure (again averaged over the 150 highest-Q eigenmodes) is also plotted, which is found to increase approximately linearly with FF.

The modal size L_{eff} decreases with FF, indicating that increasing the concentration of scatterers improves in-plane modal confinement. In the 12% – 16% FF range, where the Q factors are maximum, we obtain $L_{eff} \approx 60$ μm, which is approximately twice of the wavelength within the QC medium. For larger FFs, sub-wavelength confinement could be achieved, at the cost of lower Q factors and a reduced gain area.

Simulations have also been performed to compare modal Q factors for the present Au pillar design and a previous design based on dielectric pillars embedded in BCB[24]. For the former, we take R = 4 μm and FF = 13.6%, consistent with the discussion above. For the latter, we choose a dielectric (QC medium) pillar radius R = 6.4 μm with the same scatterer positions (thus, FF ~ 35%), so that the high-Q

"bandedge" modes are aligned with the 2.95 THz – 3.45 THz gain spectral range. In both cases, the total sample size is 500 μm × 500 μm, and eigenmodes with Q < 200 are discarded of which the optical losses cannot be compensated by the gain. **Figure 3** shows the resulting frequency distribution of the high-Q modes averaged for five different configurations.

In the dielectric pillar design, a clear bandedge effect around 3.2 THz – 3.45 THz can be observed where the mean Q factor and the number of high-Q modes are both significantly peaked. In the Au pillar design, however, the mean Q factors over the entire frequency range are as high as the highest mean Q factors achieved by the dielectric pillar counterpart. Moreover the number of high-Q modes of the Au pillar design is over 50% larger. It is also observed that for the Au pillar design, the mean Q factors and number of high-Q modes both increase slightly with frequency. This can be attributed to the higher density of optical states at higher frequencies. These results demonstrate that metal pillars are advantageous for achieving multi-mode random lasing over a broad frequency range.

In random QCLs with a dielectric pillar design, to optimize the laser performance, the scatterer size should be carefully chosen to align its "bandedge" resonance peak with the gain peak of the laser medium[17,24,34] (also see SI Text, Figure S1 and Figure S3). In the present work, there is no such requirement on the Au pillars owing to the frequency-insensitive scattering efficiency (see **Figure 1b**) and broadband property (see **Figure 1a**). As the gain is provided by the background medium (the THz QCL), it is desirable to maximize the area ratio between the gain medium and the pillars while maintaining the overall scattering strength of the random structure. Therefore, smaller scatterers with reasonable FFs are preferred, especially considering that the scattering efficiency of the smaller pillars is higher than that of the larger ones (see **Figure 1b**). In this work, the radius of the Au pillar is chosen to be 4 μm; this value is determined primarily by the difficulty of fabricating pillars with smaller radii.

To fabricate the randomly distributed Au pillars, air holes with radii ~ 4μm were etched through the QCL active region and then deposited SiO_2/Ti/Au (200 nm /30 nm /1400 nm) over the device, including on the side walls and bottom surfaces of the etched voids. As the electric field is unable to penetrate through the metal layer, each scatterer resembles a cylindrical Au pillar. The insulating gap between the bottom of each Au scatterer and the bottom contact layer is very small (~ 100 nm), so its influence on the scattering efficiency of the scatterer and the field distributions of the eigenmodes is negligible. Irregular jagged mesa boundaries were created to minimize specular refection from the edges of the sample. The light emitted from within the random cavity is extracted from emission apertures randomly etched into the top contact metal layer; these small openings have FF = 5% with radii ~ 2.5 μm, and are positioned so that they do not overlap with the scattering pillars. The small random apertures mainly work as outcouplers. As the scattering efficiency of these openings is very weak, they exert little influence on the in-plane modal localization, verified by 3D FEM simulations using Comsol Multiphysics (see SI Text, Figure S4 and S5).

The THz QCL wafer used in this work is based on a three-well resonant-phonon GaAs/ $Al_{0.15}Ga_{0.85}As$ design[35], with gain curve spanning from 2.95 THz to 3.45 THz. As the THz laser adopts subwavelength double-metal structure in the vertical direction, the optical field in the vertical direction is uniform. Therefore, 2D simulation results are instructive for the design of 3D real random metallic structures. A variety of samples were fabricated with metal pillar FFs ranging from 10% to 17%. As a reference, double-metal ridge lasers on the same QC wafer, with a size of 2 mm × 106 μm, were also fabricated and characterized. All the devices were driven by a pulser with a repetition rate of 10 kHz and a pulse width of 500 ns.

Figure 5 shows the light-current-voltage (LIV) curves and emission spectra of a random QCL with a FF of 12%. The lasing threshold at 9 K is ~ 1.53 kA/cm^2, slightly higher than that of a ridge laser (1.33

kA/cm^2). The highest working temperature is around 95 K and the peak power reaches 0.46 mW without correcting for light collection efficiency. The power performance is mainly limited by the quantum cascade wafer used, as the highest peak power achieved by the ridge laser is only 1 mW. With increasing pumping intensity, the gain spectral center of the QCL experiences a blue shift[24], which is a typical feature of the three-well resonant-phonon active region design employed here, and hence the principal emission peaks also shift towards higher frequencies. **Figure 5b** shows three complex emission spectra at different pumping currents, covering the entire dynamic range 3.05 THz – 3.45 THz, mainly limited by the gain of the QC material. More than 25 emission peaks can be observed, which is almost twice of the number of emission peaks for the previously-reported dielectric random structure, despite the fact that the present devices have only a quarter of the area[24]. Comparable emission performances are also found for the devices with different random metal pillar structures (see SI Text, Figure S7). The performance of the laser could be further improved by employing even lower-loss material, e.g., Cu[36], to replace the Au as metal pillars and top/bottom contacts in the structure.

In conclusion, we have demonstrated 2D multimode THz random QCLs with metal (Au) pillars for the first time. Metallic scatterers have previously been utilized in random lasers operating in the visible frequency range[8,16,17,37,38], thanks to the surface-plasmon enhancement of the optical scattering efficiency and the localized electromagnetic field. However, such scatterers also introduce significant light absorption, which is detrimental for practical laser devices. In the THz frequency range, by contrast, the metallic ohmic loss is almost negligible. Compared to previously-demonstrated random QCLs, the present design is notable that the metal pillars provide a high scattering efficiency over a broad spectral range for TM-polarized THz QCL light. We have observed more than 25 emission modes in the frequency range 3.05 THz – 3.45 THz, which is double that observed in previous designs, and from one quarter of the device area of the previous designs. The emission spectral range is mainly

limited by the gain bandwidth of the QC wafer. In the future, ultra-broadband random lasing (~ 1 THz) with low spatial coherence could be demonstrated by moving to QC wafers with larger gain bandwidths[26].

METHODS

Scattering efficiency calculation. The scattering efficiency is calculated by considering TM wave scattering from a cylindrically symmetric pillar. The out-of-plane electric field $\psi(\mathbf{r})$ obeys the wave equation:

$$\left[\nabla^2+\varepsilon(\mathbf{r})_{\text{rod,ext}}(\frac{\omega}{\text{c}})^2\right]\psi(\mathbf{r})=0\,, \tag{6}$$

where $\varepsilon(\mathbf{r})_{\text{rod}}$, $\varepsilon(\mathbf{r})_{\text{ext}}$ are the dielectric constants inside and outside the rod, respectively. We make the ansatz: $\psi(\mathbf{r})=\psi_{\text{inc}}(\mathbf{r})+\psi_{\text{sca}}(\mathbf{r})$, where $\psi_{\text{inc}}(\mathbf{r})\propto \text{e}^{\text{ikz}}$ is the incoming wave and $\psi_{\text{sca}}(\mathbf{r})$ is the scattered wave. By solving the above equations with boundary condition matching at $\text{r}=\text{R}$, where R is the pillar radius, the scattering efficiency can be given by:

$$\text{Q}_{\text{sca}}=\frac{\sigma_{\text{sca}}}{2\text{R}}=\frac{1}{2\text{R}}\int \text{d}\phi\left|\text{f}(\phi)\right|^2\,, \tag{7}$$

$$\text{f}(\phi)=\frac{\text{e}^{-\text{i}\pi/4}}{\sqrt{2\pi\text{k}}}\sum_{\text{m}=-\infty}^{\infty}(\text{S}_\text{m}-1)\text{e}^{\text{im}\phi}\,, \tag{8}$$

$$\text{S}_\text{m}=-\frac{\text{kJ}_\text{m}(\text{qR})\text{H}_\text{m}^{-'}(\text{kR})-\text{qJ}_\text{m}^{'}(\text{qR})\text{H}_\text{m}^{-}(\text{kR})}{\text{kJ}_\text{m}(\text{qR})\text{H}_\text{m}^{+'}(\text{kR})-\text{qJ}_\text{m}^{'}(\text{qR})\text{H}_\text{m}^{+}(\text{kR})}\,, \tag{9}$$

where $\text{q}=\sqrt{\varepsilon_{\text{rod}}}\,\omega/\text{c}$ and $\text{k}=\sqrt{\varepsilon_{\text{ext}}}\,\omega/\text{c}$.

Device Fabrication. To fabricate the THz random QCLs with Au pillars, Ti/Au (25 nm/700 nm) was first deposited both on top of the QCL structure and onto an n^+ doped GaAs host substrate; this was followed by Au/Au thermo-compression wafer bonding. The QC wafer was then polished and selectively wet-etched to remove the substrate down to an etch-stop layer. Through conventional photolithography, mask defining, and inductively coupled plasma (ICP) dry etching of the active region with a gas ratio (in SCCM) of $Ar/Cl_2/BCl_3$ = 10/5/5, the random air holes were etched through the QC wafer with the intended radius (~ 4 μm). Then, an insulation layer of 200 nm SiO_2 was deposited by a process of tetraethyl orthosilicate (TEOS) to cover the bottom and side wall of the air holes. The SiO_2 on top of the active region was then removed and a thick top contact layer (~ 25 nm/1400 nm Ti/Au) was sputtered onto the structure, guaranteeing that the random air holes were completely covered by the metal layer with a minimum thickness of 100 nm. Irregular boundaries of the top contact layer were formed by photolithography and wet etching of the metal layer. The mesa was formed by ICP with top contact metal layer as a self-aligned hard mask. Focused ion beam (FIB) etching was used to fabricate random apertures in the top contact metal layer. The etching time was carefully controlled to make sure that the semiconductor under the metal was not etched significantly. The host substrate was then thinned to around 180 μm and a 15 nm/200 nm Ti/Au layer was deposited as back contact. The samples were cleaved, indium-soldered onto copper submounts, wire-bonded and finally attached to the heatsink in a cryostat for measurement.

Device characterization. The fabricated 2D THz random QCLs with Au pillars were characterized using a FTIR spectrometer (Bruker Vertex 70 series) with a room-temperature deuterated-triglycine sulfate (DTGS) detector. The scanning resolution was 0.2 cm^{-1}. The devices were driven by a pulser with a repetition rate of 10 kHz and a pulse width of 500 ns. The devices were mounted in a helium-gas-stream cryostat for cooling with temperature control.

ASSOCIATED CONTENT

Supporting Information

Supporting Information for this article is available free of charge on the ACS Publications website at DOI: xxxxx

1). Optical properties of individual dielectric and metal pillar structure.

2). Optical properties of different random dielectric pillar structures

3). The influence of emission apertures

4). Emission performance of different random metal pillar structures

AUTHOR INFORMATION

Corresponding Author

*E-mail (Q. J. WANG): qjwang@ntu.edu.sg

Author contribution: Y. Q. Z., G. Z. L. and Q. J. W. conceived the idea; Y. Q. Z., B. Q., X. N. H., L. H. L, A. G. D., and E. H. L. performed experiment; Y. Q. Z., G. Z. L., K. D. W., J. T., and Y. D. C. performed simulation and analyzed data; Y. Q. Z., G. Z. L., Y. D. C., and Q. J. W. wrote the manuscript. K. D. W., H. K. L., and Y. Z. revised the manuscript. The authors declare no conflict of interest.

Notes

The authors declare no competing financial interest.

ACKNOWLEDGMENTS

Funding support is acknowledged from the Singapore Ministry of Education Tier 2 Program (MOE 2016-T2-1-128); Agency for Science, Technology and Research (A*STAR) (Grant No. 1426500050); Singapore National Research Foundation Competitive Research Program (NRF-CRP18-2017-02); and

the Engineering and Physical Sciences Research Council (EPSRC), UK (HyperTerahertz programme EP/P021859/1). EHL is grateful for support from the Royal Society and Wolfson Foundation. The authors are grateful to Professor Hui Cao for fruitful discussions.

REFERENCES

(1) Lawandy, N. M.; Balachandran, R. M.; Gomes, A. S. L.; Sauvain, E. Laser Action in Strongly Scattering Media. Nature **1994**, 368 (6470), 436–438.

(2) Cao, H. Lasing in Random Media. Chapter 12 **2011**, 12, 205–251.

(3) Fallert, J.; Dietz, R. J. B.; Sartor, J.; Schneider, D.; Klingshirn, C.; Kalt, H. Co-Existence of Strongly and Weakly Localized Random Laser Modes. Nat. Photonics **2009**, 3 (April), 279–282.

(4) Wiersma, D. S. Disordered Photonics. Nat. Photonics **2013**, 7 (February), 188–196.

(5) Türeci, H. E.; Ge, L.; Rotter, S.; Stone, A. D. Strong Interactions in Multimode Random Lasers. Science **2008**, 320 (5876), 643–646.

(6) Stano, P.; Jacquod, P. Suppression of Interactions in Multimode Random Lasers in the Anderson Localized Regime. Nat. Photonics **2012**, 7 (1), 66–71.

(7) Ziegler, J.; Wörister, C.; Vidal, C.; Hrelescu, C.; Klar, T. A. Plasmonic Nanostars as Efficient Broadband Scatterers for Random Lasing. **2016**, 257158.

(8) Wang, Z.; Meng, X.; Choi, S. H.; Knitter, S.; Kim, Y. L.; Cao, H.; Shalaev, V. M.; Boltasseva, A. Controlling Random Lasing with Three-Dimensional Plasmonic Nanorod Metamaterials. Nano Lett. **2016**, 16 (4), 2471–2477.

(9) Cao, H.; Zhao, Y. G.; Ho, S. T.; Seelig, E. W.; Wang, Q. H.; Chang, R. P. H. Random Laser Action in Semiconductor Powder. Phys. Rev. Lett. **1999**, 82 (11), 2278–2281.

(10) Cao, H.; Xu, J. Y.; Zhang, D. Z.; Chang, S. H.; Ho, S. T.; Seelig, E. W.; Liu, X.; Chang, R. P. H. Spatial Confinement of Laser Light in Active Random Media. Phys. Rev. Lett. **2000**, 84 (24), 5584–5587.

(11) Bahoura, M.; Morris, K. J.; Noginov, M. A. Threshold and Slope Efficiency of Nd0.5La0.5Al3 (BO3)(4) Ceramic Random Laser: Effect of the Pumped Spot Size. Opt. Commun. **2002**, 201 (4–6), 405–411.

(12) Klein, S.; Cregut, O.; Gindre, D.; Boeglin, A.; Dorkenoo, K. D. Random Laser Action in Organic Film during the Photopolymerization Process. Opt Express **2005**, 13 (14), 5387–5392.

(13) Liang, H. K.; Meng, B.; Liang, G.; Tao, J.; Chong, Y.; Wang, Q. J.; Zhang, Y. Electrically Pumped Mid-Infrared Random Lasers. Adv. Mater. **2013**, 25 (47), 6859–6863.

(14) Ruocco, G.; Abaie, B.; Schirmacher, W.; Mafi, A.; Leonetti, M. Disorder-Induced Single-Mode Transmission. Nat. Commun. **2017**, 8, 14571.

(15) Fan, S. Z.; Zhang, X. Y.; Wang, Q. P.; Zhang, C.; Wang, Z. P. Build-up Time of the Random Laser in R6G Dye Solution with TiO(2) Scatterers. High-Power Lasers Appl. V **2010**, 7843, 784314.

(16) Dice, G. D.; Mujumdar, S.; Elezzabi, A. Y. Plasmonically Enhanced Diffusive and Subdiffusive Metal Nanoparticle-Dye Random Laser. Appl. Phys. Lett. **2005**, 86 (13), 1–3.

(17) Popov, O.; Zilbershtein, A.; Davidov, D. Random Lasing from Dye-Gold Nanoparticles in Polymer Films: Enhanced Gain at the Surface-Plasmon-Resonance Wavelength. Appl. Phys. Lett. **2006**, 89 (19), 8–11.

(18) Marini, A.; García de Abajo, F. J. Graphene-Based Active Random Metamaterials for Cavity-Free Lasing. Phys. Rev. Lett. **2016**, 116 (21), 217401.

(19) Polson, R. C.; Vardeny, Z. V. Random Lasing in Human Tissues. Appl. Phys. Lett. **2004**, 85 (7), 1289–1291.

(20) Redding, B.; Choma, M. A.; Cao, H. Speckle-Free Laser Imaging Using Random Laser Illumination. Nat. Photonics **2012**, 6 (6), 355–359.

(21) Liang, H. K.; Meng, B.; Liang, G. Z.; Tao, J.; Chong, Y. D.; Wang, Q. J.; Zhang, Y. Electrically Pumped Mid-Infrared Random Lasers. Adv. Mater. **2013**, 25 (47), 6859–6863.

(22) Schönhuber, S.; Brandstetter, M.; Hisch, T.; Deutsch, C.; Krall, M.; Detz, H.; Andrews, A. M.; Strasser, G.; Rotter, S.; Unterrainer, K. Random Lasers for Broadband Directional Emission. Optica **2016**, 3 (10), 1035.

(23) Degl'Innocenti, R.; Shah, Y. D.; Masini, L.; Ronzani, A.; Pitanti, A.; Ren, Y.; Jessop, D. S.; Tredicucci, A.; Beere, H. E.; Ritchie, D. A. Hyperuniform Disordered Terahertz Quantum Cascade Laser. Sci. Rep. **2016**, 6 (1), 19325.

(24) Zeng, Y.; Liang, G.; Liang, H. K.; Mansha, S.; Meng, B.; Liu, T.; Hu, X.; Tao, J.; Li, L.; Davies, A. G.; Linfield, E. H.; Zhang, Y.; Chong, Y.; Wang, Q. J. Designer Multimode Localized Random Lasing in Amorphous Lattices at Terahertz Frequencies. ACS Photonics **2016**, 3 (12), 2453–2460.

(25) Smith, D. R.; Schultz, S.; Kroll, N.; Sigalas, M.; Ho, K. M.; Soukoulis, C. M. Experimental and Theoretical Results for a Two-Dimensional Metal Photonic Band-Gap Cavity. Appl. Phys. Lett. **1994**, 65 (5), 645–647.

(26) Turčinková, D.; Scalari, G.; Castellano, F.; Amanti, M. I.; Beck, M.; Faist, J.; Turc, D. Ultra-Broadband Heterogeneous Quantum Cascade Laser Emitting from 2 . 2 to 3 . 2 THz. **2016**, 191104 (2011), 97–100.

(27) Zhao, Y.; Grischkowsky, D. R. 2-D Terahertz Metallic Photonic Crystals in Parallel-Plate Waveguides. IEEE Trans. Microw. Theory Tech. **2007**, 55 (4), 656–663.

(28) Bayindir, M.; Cubukcu, E.; Bulu, I.; Tut, T.; Ozbay, E.; Soukoulis, C. Photonic Band Gaps, Defect Characteristics, and Waveguiding in Two-Dimensional Disordered Dielectric and Metallic Photonic Crystals. Phys. Rev. B **2001**, 64 (19), 1–7.

(29) Ordal, M. A.; Long, L. L.; Bell, R. J.; Bell, S. E.; Bell, R. R.; Alexander, R. W.; Ward, C. A. Optical Properties of the Metals Al, Co, Cu, Au, Fe, Pb, Ni, Pd, Pt, Ag, Ti, and W in the Infrared and Far Infrared. Appl. Opt. **1983**, 22 (7), 1099.

(30) Sebbah, P.; Vanneste, C. Random Laser in the Localized Regime. Phys. Rev. B **2002**, 66 (14), 1–10.

(31) Faist, J.; Capasso, F.; Sivco, D. L.; Sirtori, C.; Hutchinson, A. L.; Cho, A. Y. Quantum Cascade Laser. Science (80-.). **1994**, 264 (5158), 553–556.

(32) Kong, J. A. Electromagnetic Wave Theory. 1986, p 696.

(33) Schwartz, T.; Bartal, G.; Fishman, S.; Segev, M. Transport and Anderson Localization in Two-Dimensional Photonic Lattices. Nature **2007**, 446 (March), 52–55.

(34) Gottardo, S.; Sapienza, R.; García, P. D.; Blanco, A.; Wiersma, D. S.; López, C. Resonance-Driven Random Lasing. Nat. Photonics **2008**, 2 (7), 429–432.

(35) Belkin, M.; Wang, Q.; Pflügl, C.; Belyanin, A.; Khanna, S. P.; Davies, A. G.; Linfiel, E. H.; Capasso, F. High-Temperature Operation of Terahertz Quantum Cascade Laser Sources. IEEE J. Sel. Top. Quantum Electron. **2009**, 15 (3), 952–967.

(36) Belkin, M. A.; Fan, J. A.; Hormoz, S.; Capasso, F.; Khanna, S. P.; Lachab, M.; Davies, A. G.; Linfield, E. H. Terahertz Quantum Cascade Lasers with Copper Metal-Metal Waveguides Operating up to 178 K. Opt Express **2008**, 16 (5), 3242–3248.

(37) Zhai, T.; Zhang, X.; Pang, Z.; Su, X.; Liu, H.; Feng, S.; Wang, L. Random Laser Based on Waveguided Plasmonic Gain Channels. Nano Lett. **2011**, 11 (10), 4295–4298.

(38) Meng, X.; Fujita, K.; Moriguchi, Y.; Zong, Y.; Tanaka, K. Metal-Dielectric Core-Shell Nanoparticles: Advanced Plasmonic Architectures Towards Multiple Control of Random Lasers. Adv. Opt. Mater. **2013**, 1 (8), 538–538.

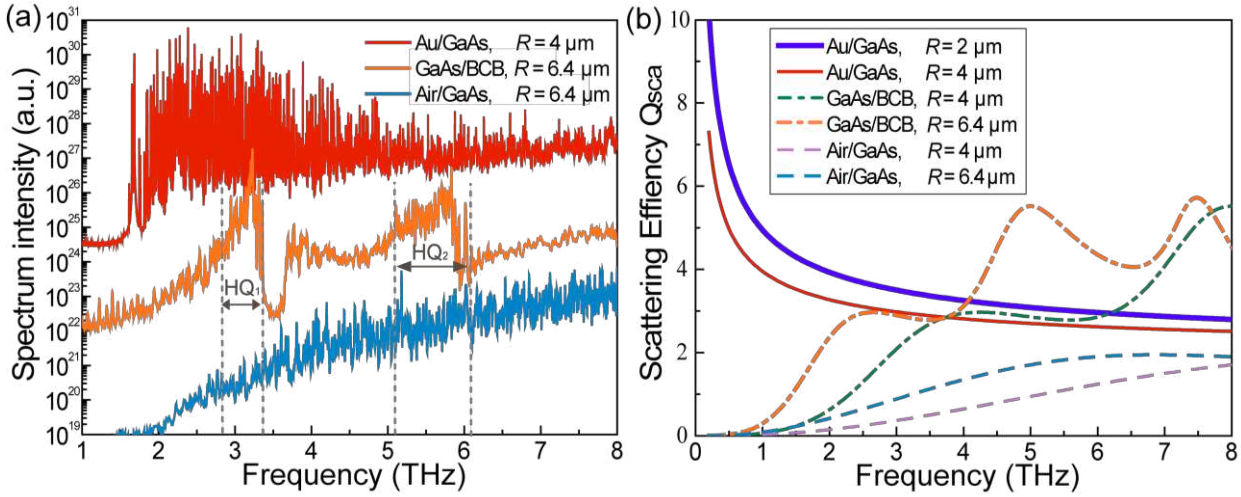

Figure 1. Optical power spectra and scattering efficiency analysis of random structures. (a) Simulated optical power spectra (vertically offset for clarity) of three 2D random structures: Au pillars embedded in GaAs, GaAs pillars in benzocyclobutene (BCB) polymer, and air holes in GaAs. In three cases, 680 pillars or holes have identical random placement without scatterer overlapping, in a square cell of area 500 μm × 500 μm. The circular scatterers have different radii, i.e., 4 μm for the Au pillars, and 6.4 μm for the dielectric pillars and air holes. Gray dashed line indicates the high-Q resonance frequency range (HQ_1 and HQ_2) of disordered dielectric pillar lattice. (b) The scattering efficiency Q_{sca} (defined as the ratio of scattering cross section to the scatterer diameter) as a function of frequency for individual Au pillars, GaAs pillars, and air holes of various sizes.

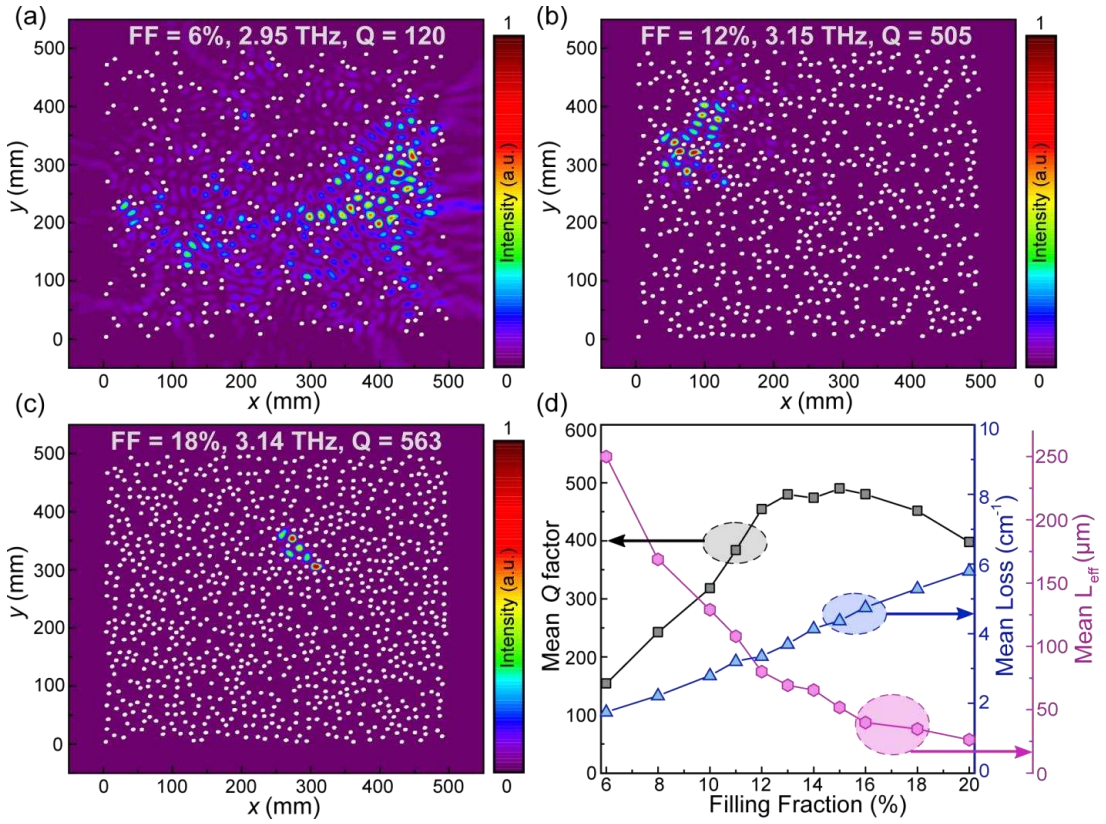

Figure 2. Simulated field distributions in 2D disordered lattices of Au pillars. (a)–(c) Normalized field intensity distributions for typical high-Q modes for pillar FF of (a) 6%, (b) 12%, and (c) 18%. The white circles indicate the Au pillars, which have radius R = 4 μm and are randomly distributed with no overlap within a 500 μm × 500 μm area. A perfectly matched layer was used to eliminate the reflection from the simulation domain boundaries. (d) Mean Q factors, effective modal sizes, and ohmic losses as a function of pillar FF. These quantities are averaged over the 150 highest-Q modes within the 2.95 THz – 3.45 THz spectral range, for five independent sample configurations per FF.

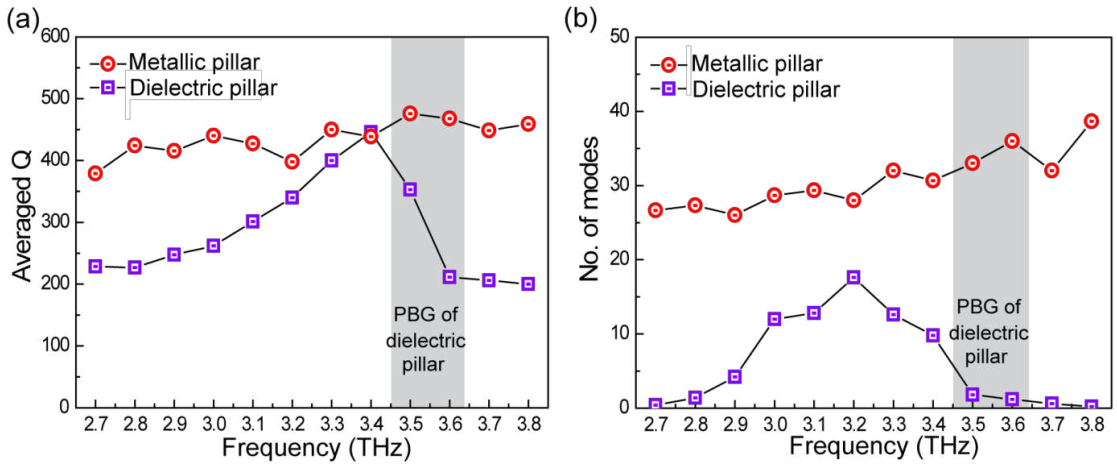

Figure 3. Frequency distribution of modal Q factors in disordered metal pillar and disordered dielectric pillar lattices. (a) Mean Q factors (for modes with Q > 200) as a function of frequency. (b) The number of eigenmodes with Q > 200 as a function of frequency. The frequencies are binned at 0.1 THz intervals. Results are shown for Au pillars in GaAs, with pillar radius R = 4 μm and 13.6% FF (red circles), and GaAs pillars in BCB, with pillar radius 6.4 μm and 35% FF (purple squares); in both cases, the pillars are distributed within a 500 μm × 500 μm area. The pseudo-gap of the dielectric pillar lattice is highlighted in gray. The high-Q eigenmode quantities are averaged over five configurations.

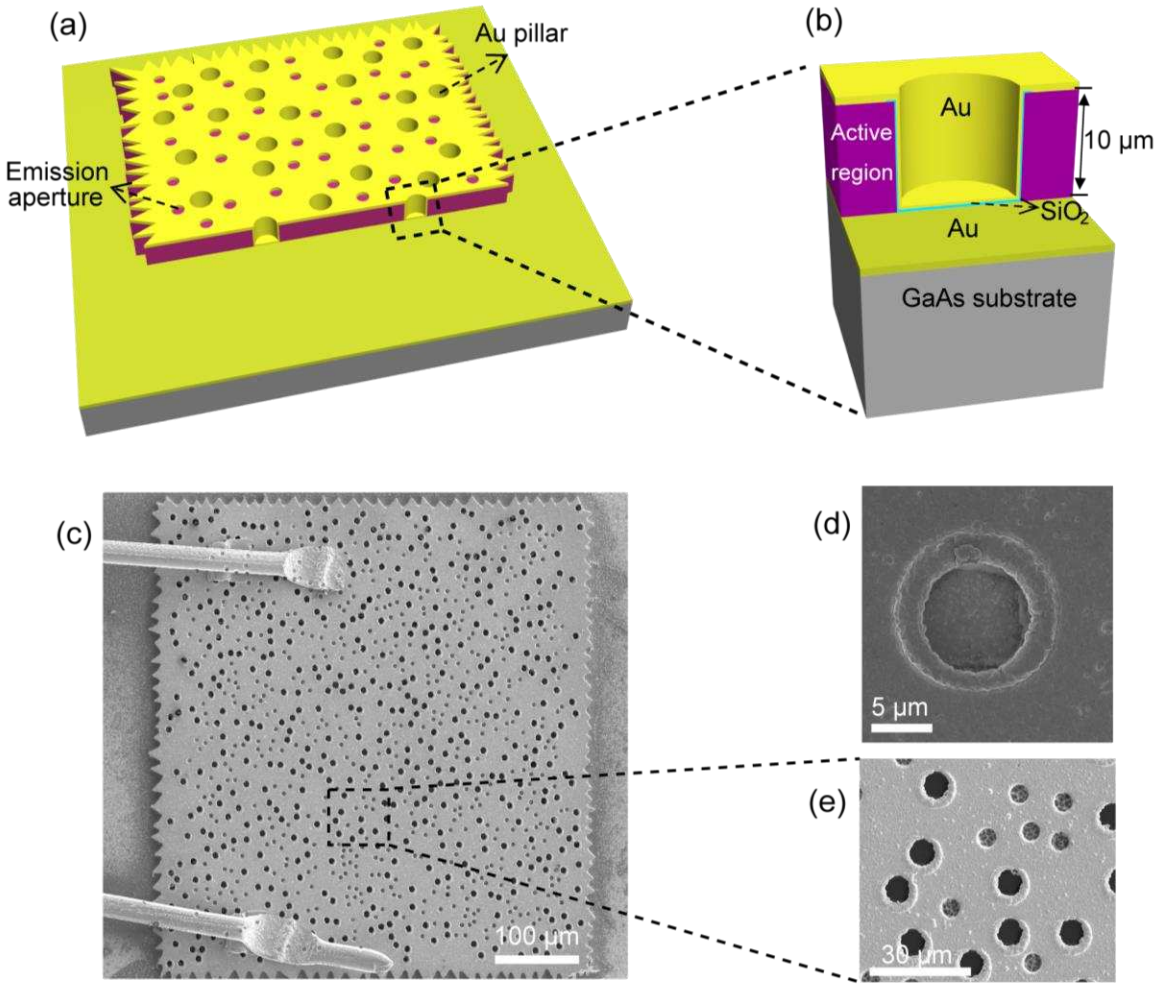

Figure 4. THz random quantum cascade laser (QCL) with metal pillars. (a) Schematic illustration of the device. (b) Detail of a single pillar scatterer. (c) Scanning electron microscope (SEM) images of the fabricated device, with (d) detail of a single metal pillar, imaged at an oblique angle, and (e) detail of metal pillars and emission apertures etched into the top metal contact. It can be seen that the air hole etched through the QCL active region is completely covered by metal.

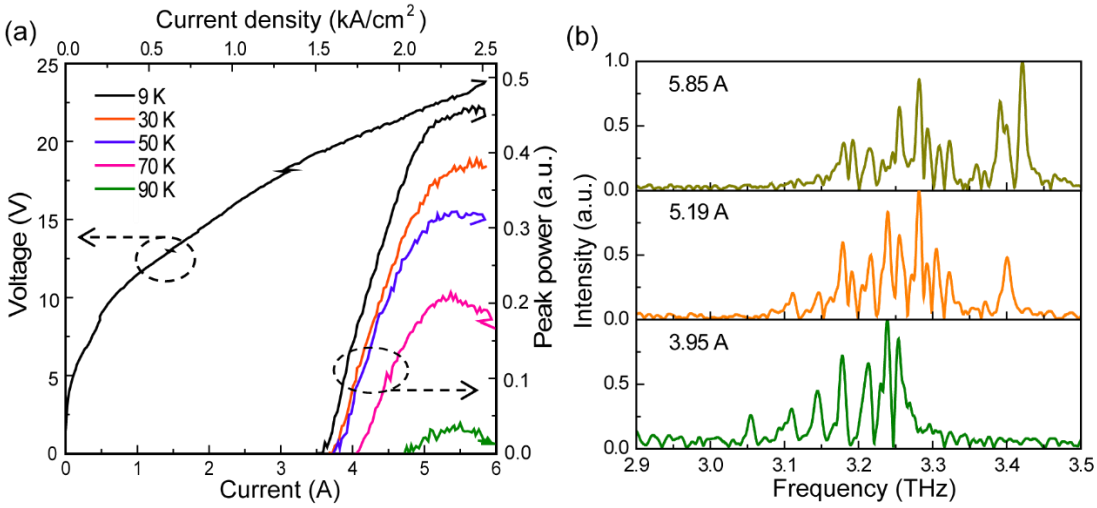

Figure 5. Emission characteristics of a THz random QCL with metal pillars. (a) Light-current-voltage (LIV) curves at different temperatures and (b) emission spectra at 9 K for different pumping currents of the THz random QCL. The total structure size is around 515 µm × 515 µm and the FF of the gold pillars is 12%. The laser is operated in pulsed mode with a repetition rate of 10 kHz and a pulse width of 500 ns.